Mon. Not. R. Astron. Soc. **000**, 000–000 (0000) Printed March 9, 2016 (MN LATEX style file v2.2)

Tapering the sky response for angular power spectrum estimation from low-frequency radio-interferometric data

Samir Choudhuri[1⋆], Somnath Bharadwaj[1]†, Nirupam Roy[1], Abhik Ghosh[2] and Sk. Saiyad Ali[3]

[1] *Department of Physics, & Centre for Theoretical Studies, IIT Kharagpur, Kharagpur 721 302, India*
[2] *Kapteyn Astronomical Institute, PO Box 800, 9700 AV Groningen, The Netherlands*
[3] *Department of Physics,Jadavpur University, Kolkata 700032, India*

arXiv:1603.02513v1 [astro-ph.CO] 8 Mar 2016

ABSTRACT

It is important to correctly subtract point sources from radio-interferometric data in order to measure the power spectrum of diffuse radiation like the Galactic synchrotron or the Epoch of Reionization 21-cm signal. It is computationally very expensive and challenging to image a very large area and accurately subtract all the point sources from the image. The problem is particularly severe at the sidelobes and the outer parts of the main lobe where the antenna response is highly frequency dependent and the calibration also differs from that of the phase center. Here we show that it is possible to overcome this problem by tapering the sky response. Using simulated 150 MHz observations, we demonstrate that it is possible to suppress the contribution due to point sources from the outer parts by using the Tapered Gridded Estimator to measure the angular power spectrum C_ℓ of the sky signal. We also show from the simulation that this method can self-consistently compute the noise bias and accurately subtract it to provide an unbiased estimation of C_ℓ.

Key words: methods: statistical, data analysis - techniques: interferometric- cosmology: diffuse radiation

1 INTRODUCTION

Foreground removal for detecting the Epoch of Reionization (EoR) 21-cm signal is a topic of intense current research (Jelić et al. 2008; Bowman, Morales & Hewitt 2009; Paciga et al. 2011; Chapman et al. 2012; Liu & Tegmark 2012; Mao 2012; Paciga et al. 2013). Foreground avoidance (Datta et al. 2010; Parsons et al. 2012; Trott et al. 2012; Vedantham et al. 2012; Pober et al. 2013; Thyagarajan et al. 2013; Parsons et al. 2014; Dillon et al. 2014; Pober et al. 2014; Liu et al. 2014a,b; Ali et al. 2015) is an alternate strategy based on the proposal that the foreground contamination is restricted to a wedge in $(k_\perp, k_\parallel)$ space, and the signal can be estimated from the uncontaminated modes outside the wedge. Point sources dominate the 150 MHz sky at the angular scales $\leq 4^\circ$ (Ali, Bharadwaj & Chengalur 2008) which are relevant for telescopes like the Giant Metrewave Radio Telescope (GMRT; Swarup et al. 1991), Low-Frequency Array (LOFAR; van Haarlem et al. 2013) and the upcoming Square Kilometre Array[1] (SKA). It is difficult to model and subtract the point sources at the periphery of the telescope's field of view. The difficulties include the fact that the antenna response is highly frequency dependent near the nulls of the primary beam, and the calibration differs from that of the phase center due to ionospheric fluctuations. Point source subtraction is also important for measuring the angular power spectrum of the diffuse Galactic synchrotron radiation (Bernardi et al. 2009; Ghosh et al. 2012; Iacobelli et al. 2013) which, apart from being an important foreground component for the EoR 21-cm signal, is interesting in its own right.

Most of the foreground subtraction techniques use the property of smoothness along frequency for the various foreground components. Ghosh et al. (2011a,b) found that residual point sources located away from the phase center introduce oscillations along frequency direction. The oscillation are more rapid if the distance of the source from the phase center increases, and also with increasing baseline. Equivalently, the dominant contribution to the width of the foreground wedge arises from the sources located at the periphery of the field of view (Thyagarajan et al. 2013). Using GMRT Ghosh et al. (2011b, 2012) have shown that these oscillations can be reduced by tapering the sky response. In a recent paper Pober et al. (2016) showed that correctly

⋆ Email:samir11@phy.iitkgp.ernet.in
† Email:somnath@phy.iitkgp.ernet.in
[1] https://www.skatelescope.org

modelling and subtracting the sidelobe foreground contamination is important for detecting the redshifted 21-cm signal.

In a recent paper Choudhuri et al. (2014) have introduced the Tapered Gridded Estimator (TGE) for estimating the angular power spectrum C_ℓ directly from radio-interferometric visibility data. In this paper we use simulated 150 MHz GMRT data which incorporates point sources and the diffuse Galactic synchrotron radiation to demonstrate that it is possible to suppress the contribution from residual point sources in the sidelobes and the outer parts of the primary beam in estimating C_ℓ using the TGE.

Noise bias is an important issue for any estimator. For example, the image based estimator (Seljak 1997) for C_ℓ and the visibility based estimator (Liu & Tegmark 2012) for $P(k_\perp, k_\parallel)$ rely on modelling the noise properties of the data and subtracting out the expected noise bias. However, the actual noise in the observations could have baseline, frequency and time dependent variations which are very difficult to model and there is the risk of residual noise bias being mistaken as the signal. Paciga et al. (2011) have avoided the noise bias by cross-correlating observations made on different days. Another visibility based estimator (Begum et al. 2006; Dutta et al. 2007) individually correlates pairs of visibilities avoiding the self correlation that is responsible for the noise bias. This, however, is computationally very expensive when the data volume is large. In this paper, we have demonstrated that TGE, by construction, estimates the actual noise bias internally from the data and exactly subtracts this out to give an unbiased estimate of C_ℓ. The entire discussion here is in the context of estimating C_ℓ for the diffuse Galactic synchrotron radiation. As mentioned earlier, the same issues are also relevant for measuring the EoR 21-cm power spectrum not considered here.

In Section 2 we discuss the conventional problem in standard imaging techniques. Simulation and data analysis processes are briefly discussed in Section 3. Section 4 discusses the estimator (TGE) that we used to suppress the outer region of the primary beam and the results are presented in Section 5. Finally, we present summary and conclusion in Section 6.

2 PROBLEMS IN CONVENTIONAL IMAGING

The contribution to the signal in radio frequency observations from the outer region of the primary beam and from the sidelobes is generally very small as compared to the inner region of the primary beam. In particular, the expected 21-cm signal, which itself is very faint, contributes mainly from the central part of the primary beam, and attenuated to a great extent in the outer region. Only the bright point sources from the outer region, if not accurately removed, may have significant impact on the statistical estimation of the diffuse signal. Thus, it is necessary to remove the effect of point sources from the outer region before estimating the residual power spectrum. However, we will not be benefitted in terms of signal by including highly attenuated diffuse emission from the outer region.

Imaging a large enough region to model and subtract all the point sources before dealing with the diffuse emission may seems to be a direct solution of the above problem. But, in reality there are many issues which make this approach impractical. First of all, the field of view at low radio frequencies is large, and making larger images is computationally more expensive. In addition to that, non-coplaner nature of the baselines prevents us from making wide-field image without considering the effect of the "w-term". There are algorithms e.g. faceting (Cornwell & Perley 1992), w-projection (Cornwell et al. 2008), WB-A projection (Bhatnagar et al. 2013) etc. to tackle this problem partly for radio interferometric observations. However, these algorithms still require significant computation to make an image of such a large region of the sky. Secondly, the number of bright point sources is quite large at low frequency. While imaging a very large region, selecting CLEANing region around each source is a tedious job. On the other hand, CLEANing without selecting regions removes a non-negligible part of the diffuse signal of our interest (see Choudhuri et al. 2016, for details).

The next challenge is to accurately characterize the time and frequency dependence of the wide-field primary beam for effective point source subtraction from the periphery of the telescope's field of view (e.g. Neben et al. 2015). Both the frequency dependence and the deviation from circular symmetry are more prominent at the outer part of the primary beam. These, along with the rotation of primary beam on the sky, cause a strong time and frequency variation of the primary beam for point sources in the outer region. They create problem in accurately model the point sources that we want to subtract from the data. In fact, some of the variations are intractable in nature and it is extremely difficult, if not impossible, to make accurate modelling and subtraction of the point sources from the outer part of the primary beam.

Though we have not considered instrumental gains and ionospheric effects in this study, in real life any directional dependence of these quantities will also severely limit our ability to subtract point sources accurately from a large region. One can overcome this difficulty to some extent by going into complicated and messy procedure of direction dependent calibration (e.g. peeling) (Bhatnagar et al. 2008; Intema et al. 2009; Kazemi et al. 2011). Again, (a) it is computationally more expensive, (b) part of the variation may be intractable, and (c) there is hardly any gain in terms of recovering the diffuse signal which is too weak in outer region.

The future generation low frequency telescopes (e.g. SKA) that will presumably be used to carry out redshifted diffuse H I observation, will have larger field of view, large bandwidth, longer baseline and higher sensitivity. Hence the above issues will be even more relevant. Moreover, the expected huge data volume from observations with those telescopes will make it more challenging to address these problems by imaging a larger region for subtracting the point sources. The following two sections outline a technique to overcome these problems by subtracting point sources only from the central region and using the TGE to recover the power spectrum of the diffuse emission in a more efficient way.

3 SIMULATION AND DATA ANALYSIS

The details of the simulation and data analysis, including point source subtraction, are presented in a companion pa-

per (Choudhuri et al. 2016) and we only present a brief discussion here. Our model of the 150 MHz sky has two components, the first being the diffuse Galactic synchrotron radiation which is the signal that we want to detect. We use the measured angular power spectrum (Ghosh et al. 2012)

$$C_\ell^M(\nu) = A_{150} \times \left(\frac{1000}{\ell}\right)^\beta \times \left(\frac{\nu}{150\mathrm{MHz}}\right)^{-2\alpha} . \quad (1)$$

as the input model to generate the brightness temperature fluctuations on the sky. Here ν is the frequency in MHz, $A_{150} = 513\,\mathrm{mK}^2$, $\beta = 2.34$ (Ghosh et al. 2012) and $\alpha = 2.8$ (Platania et al. 1998). The simulation covers a $\sim 8^\circ \times \sim 8^\circ$ region of the sky and a 16 MHz bandwidth, centered at 150 MHz, over 128 spectral channels. The diffuse signal was simulated on a grid of resolution $\sim 0.5^{'}$.

The Poisson fluctuation of the extragalactic point sources dominates the 150 MHz sky at the angular scales of our interest (Ali, Bharadwaj & Chengalur 2008), and it is necessary to subtract these or suppress their contribution in order to detect any diffuse component like the Galactic synchrotron radiation which we consider here or the redshifted 21-cm cosmological signal which is much fainter and is not considered here. We use the 150 MHz differential source count measured using GMRT (Ghosh et al. 2012)

$$\frac{dN}{dS} = \frac{10^{3.75}}{Jy \cdot Sr} \cdot \left(\frac{S}{1Jy}\right)^{-1.6} . \quad (2)$$

to generate point sources in the flux range 9mJy to 1Jy whose angular positions are randomly distributed within the $3.1^\circ \times 3.1^\circ$ Full Width Half Maxima (hereafter FWHM) of the primary beam. The antenna response falls off beyond the FWHM, and we only include the bright sources ($S \geq$ 100mJy) outside the FWHM. We have 353 and 343 sources in the inner and outer regions respectively, and the sources were assigned a randomly chosen spectral index α ($S_\nu \propto \nu^{-\alpha}$) in the range 0.7 to 0.8.

We consider the mock GMRT observations targeted on a arbitrarily selected field located at RA=10h 46m 00s and DEC=59° 00′ 59″. The GMRT has 30 antennas which for a total 8 hr of observation with 16s integration time results in 783,000 baselines $\mathbf{U}_i$ with 128 visibilities $\mathcal{V}(\mathbf{U}_i, \nu)$ (one per frequency channel) for each baseline. The resolution of GMRT at 150 MHz is 20″. The diffuse signal (eq. 1) falls off with increasing $U = \mid \mathbf{U} \mid (\ell = 2\pi U)$, and we include this contribution for only the small baselines $U \leq 3,000$ for which the visibility contribution is calculated using a 2 dimensional Fourier transform. We note that the w term does not significantly affect the diffuse signal (Choudhuri et al. 2014), however this is very important for correctly imaging and subtracting the point sources. We have included the point source contribution for all the baselines in the simulation, and the visibilities are calculated by individually summing over each point source and including the w term. We have modelled the GMRT primary beam pattern $\mathcal{A}(\vec{\theta}, \nu)$ with the square of a Bessel function (Figure 1) corresponding to the telescope's 45 m diameter circular aperture. The simulated sky is multiplied with $\mathcal{A}(\vec{\theta}, \nu)$ before calculating the visibilities. Finally, we add the system noise contribution which is modelled a Gaussian random variable with standard deviation $\sigma_n = 1.03$Jy for the real and imaginary parts of each visibility. We note that the GMRT has two polarizations which have identical sky signals but independent noise.

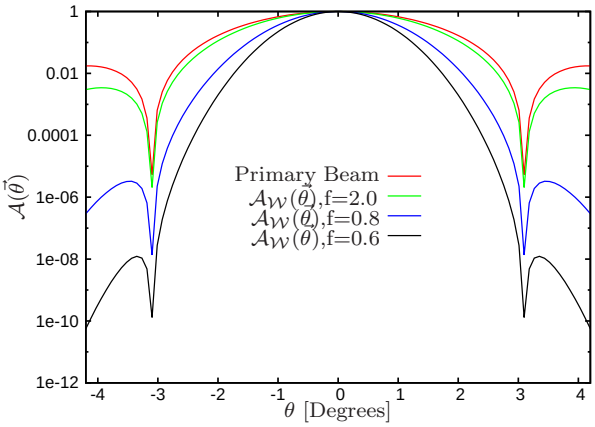

Figure 1. The GMRT 150 MHz primary beam $\mathcal{A}(\vec{\theta})$ which has been modelled as the square of a Bessel function. The effective primary beam $\mathcal{A}_\mathcal{W}(\vec{\theta})$, obtained after tapering the sky response for the different values of f is also shown in the figure.

We have used the Common Astronomy Software Applications (CASA)[2] package to image and analyze our simulated data. The standard tasks CLEAN and UVSUB were used to model and subtract out the point sources from a $4.2^\circ \times 4.2^\circ$ region which covers an extent that is approximately 1.5 times the FWHM of the primary beam. We have tried different CLEAN strategies for which the details are presented in our companion paper (Choudhuri et al. 2016), and for this work we adopt the most optimum parameter values which correspond to Run(e) of the companion paper. Figure 2 shows the "dirty" image of the entire simulation region made from the residual visibility data after point source subtraction. The central square box ($4.2^\circ \times 4.2^\circ$) shows the region from which the point sources have been subtracted. The features visible in this region correspond to the Galactic synchrotron radiation. It is difficult to model and subtract point sources from the periphery where the antenna response is highly frequency dependent. It also needs creating and cleaning a huge image that is computationally more expensive. Further, in real observations, any direction dependent gain away from the phase center will make it even more difficult. We have not attempted to subtract the point sources from the region outside the central box and the residual point sources are visible in this region of the image.

Figure 3 shows the angular power spectrum C_ℓ before and after point source subtraction; the input model for the diffuse radiation is also shown for comparison. Before subtraction, the point sources dominate C_ℓ at all angular multipoles ℓ. After subtraction, we are able to recover the diffuse component at low angular multipoles $\ell \leq 3 \times 10^3$. However, the residual point sources still dominate at the large ℓ values. The goal is to suppress the contribution from the residual point sources located at the periphery of the beam so that we can recover the input model over the entire ℓ range. We show that it is possible to achieve this with the Tapered Gridded Estimator discussed in the next section.

[2] http://casa.nrao.edu/

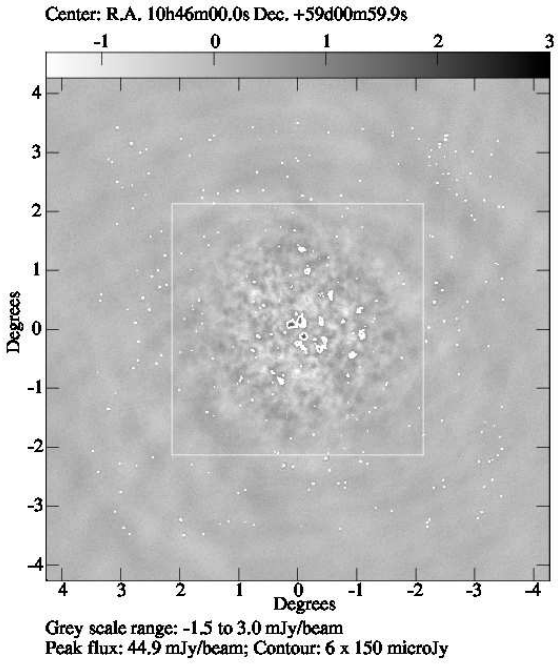
Center: R.A. 10h46m00.0s Dec. +59d00m59.9s
Degrees
Degrees
Grey scale range: -1.5 to 3.0 mJy/beam
Peak flux: 44.9 mJy/beam; Contour: 6 x 150 microJy

Figure 2. "Dirty" image of the entire simulation region made with the residual visibility data after point source subtraction. Point sources were subtracted from a central region (shown with a box, $4.2^\circ \times 4.2^\circ$) whose extent is ~ 1.3 times the FWHM of the primary beam. The features visible inside the box all correspond to the diffuse radiation. Residual point sources are visible outside the box, however the diffuse radiation is not visible in this region.

4 THE TAPERED GRIDDED ESTIMATOR

The observed visibilities are a sum of two independent parts namely the sky signal and the system noise

$$\mathcal{V}(\mathbf{U},\nu) = \mathcal{S}(\mathbf{U},\nu) + \mathcal{N}(\mathbf{U},\nu)\,. \tag{3}$$

The signal $\mathcal{S}(\mathbf{U},\nu)$ and the noise $\mathcal{N}(\mathbf{U},\nu)$ are considered to be independent random variables, further the noise in the different visibilities are uncorrelated. The signal contribution $\mathcal{S}(\mathbf{U},\nu)$ records the Fourier transform of the product of $\delta I(\vec{\theta},\,\nu)$, the fluctuation in specific intensity of the sky signal, and the telescope's primary beam pattern $\mathcal{A}(\theta,\nu)$ shown in Figure 1. As mentioned earlier, it is difficult to model and subtract point sources from the outer region of the primary beam and the sidelobes. The residual point sources in the periphery of the telescope's field of view pose a problem for estimating the power spectrum of the diffuse radiation. In this section we discuss the Tapered Gridded Estimator (TGE) which is a technique for estimating the angular power spectrum from the visibility data. This technique suppresses the contribution from the sidelobes and the outer part of the primary beam by tapering the sky response. Choudhuri et al. (2014) presents a detailed discussion of this estimator, and we only present a brief outline here.

We taper the sky response by multiplying the field of view with a frequency independent Gaussian window function $\mathcal{W}(\theta) = e^{-\theta^2/\theta_w^2}$. Here we parametrize $\theta_w = f\theta_0$ where $\theta_0 = 0.6 \times \theta_{FWHM}$ and θ_{FWHM} is the FWHM of the telescope's primary beam at the central frequency, and preferably $f \leq 1$ so that $\mathcal{W}(\theta)$ cuts off the sky response well before the first null of the primary beam. We implement the tapering by convolving the measured visibilities with $\tilde{w}(\mathbf{U})$ the Fourier transform of $\mathcal{W}(\theta)$. The convolved visibilities are evaluated on a grid in uv space using

$$\mathcal{V}_{cg} = \sum_i \tilde{w}(\mathbf{U}_g - \mathbf{U}_i)\,\mathcal{V}_i \tag{4}$$

where $\mathbf{U}_g$ refers to the different grid points and $\mathcal{V}_i$ refers to the measured visibilities at baseline $\mathbf{U}_i$. The gridding significantly reduces the data volume and the computation time required to estimate the power spectrum (Choudhuri et al. 2014). The convolved visibilities are calculated separately for each frequency channel. Then, for the purpose of this work, convolved visibilities for a grid are averaged over all frequencies.

The signal component of the convolved visibility is the Fourier transform of the product of a modified primary beam pattern $\mathcal{A}_W(\vec{\theta},\nu) = \mathcal{W}(\theta)\,\mathcal{A}(\vec{\theta},\nu)$ and $\delta I(\vec{\theta},\nu)$

$$\mathcal{S}_c(\mathbf{U},\nu) = \int d^2\vec{\theta}\,\mathcal{A}_W(\theta,\nu)\delta I(\vec{\theta},\,\nu)e^{2\pi i\mathbf{U}.\vec{\theta}}\,. \tag{5}$$

It is clear that the convolved visibilities respond to the signal from a smaller region of the sky as compared to the measured visibilities. It may be noted that the tapering is effective only if the window function $\tilde{w}(\mathbf{U}_g - \mathbf{U}_i)$ in eq. (4) is well sampled by the baseline distribution. The results of this paper, presented later, indeed justify this assumption for the GMRT.

The correlation of the gridded visibilities $\langle \mathcal{V}_{cg}\mathcal{V}^*_{cg}\rangle$ gives a direct estimate of the angular power spectrum C_{ℓ_g} through

$$\langle \mathcal{V}_{cg}\mathcal{V}^*_{cg}\rangle = \mid K_{1g} \mid^2 V_1 C_{\ell_g} + \sum_i \mid \tilde{w}(\mathbf{U}_g - \mathbf{U}_i) \mid^2 \langle \mid \mathcal{N}_i \mid^2 \rangle \tag{6}$$

where the angular multipole ℓ_g is related to the baseline U_g as $\ell_g = 2\pi U_g$, $K_{1g} = \sum_i \tilde{w}(\mathbf{U}_g - \mathbf{U}_i)$, $V_1 = \left(\frac{\partial B}{\partial T}\right)^2 \left[\int d^2U' \mid \tilde{a}_W(\mathbf{U} - \mathbf{U}') \mid^2\right]$, $\tilde{a}_W$ is the Fourier transform of $\mathcal{A}_W$ and $\left(\frac{\partial B}{\partial T}\right)$ is the conversion factor from brightness temperature to specific intensity. We see that the visibility correlation also has a term involving $\langle \mid \mathcal{N}_i \mid^2 \rangle$ which is the variance of the noise contribution present in the measured visibilities (eq. 3). This term, which is independent of C_ℓ, introduces a positive definite noise bias. The visibility correlation (eq. 6) provides an estimate of C_ℓ except for the additive noise bias. The TGE uses the same visibility data to obtain an internal estimate of the noise bias and subtract it from the visibility correlation. We consider the self-correlation term $B_{cg} = \sum_i \mid \tilde{w}(\mathbf{U}_g - \mathbf{U}_i) \mid^2 \mid \mathcal{V}_i \mid^2$ for which

$$\langle B_{cg}\rangle = \sum_i \mid \tilde{w}(\mathbf{U}_g - \mathbf{U}_i) \mid^2 (V_0 C_{\ell_i} + \langle \mid \mathcal{N}_i \mid^2 \rangle)\,. \tag{7}$$

where $V_0 = \left(\frac{\partial B}{\partial T}\right)^2 \left[\int d^2U' \mid \tilde{a}(\mathbf{U} - \mathbf{U}') \mid^2\right]$, $\tilde{a}$ is the Fourier transform of the primary beam pattern $\mathcal{A}$. The term $\langle B_{cg}\rangle$, by construction, has exactly the same noise bias as the visibility correlation in eq. (6). We use this to define the TGE estimator

$$\hat{E}_g = (\mid K_{1g} \mid^2 V_1)^{-1}[\mathcal{V}_{cg}\mathcal{V}^*_{cg} - B_{cg}] \tag{8}$$

which gives an unbiased estimate of the angular power spectrum at a grid point g. A part of the signal also gets subtracted out with the noise bias. This loss is proportional to

N (the number of visibility data) whereas the visibility correlation is proportional to N^2, and this loss is insignificant when the data size is large (Choudhuri et al. 2014). The C_{ℓ_g} values estimated at each grid point are binned in logarithmic intervals of ℓ, and we consider the bin-averaged C_ℓ as a function of the bin-averaged angular multipole ℓ.

Tapering reduces the sky coverage which, in addition to suppressing the point sources in the periphery of the main lobe and the sidelobes, also affects the diffuse signal. The reduced sky coverage causes the cosmic variance of the estimated C_ℓ to increase as f is reduced (Figure 10, Choudhuri et al. 2014). Further, the reduced sky coverage also restricts the ℓ range ($\ell_{min} - \ell_{max}$) where it is possible to estimate C_ℓ, and the value of ℓ_{min} increases as f is decreased.

5 RESULTS

We have applied the Tapered Gridded Estimator (TGE) to the residual visibility data after subtracting out the point sources. As mentioned earlier, the point sources have been identified and subtracted from a $4.2^\circ \times 4.2^\circ$ region (Figure 2) which covers an extent that is ≈ 1.3 times the FWHM of the primary beam. However, the point sources still remain at the periphery of the primary beam and in the part of the sidelobe which has been included in the simulation. The TGE tapers the sky response which results in an effective primary beam $\mathcal{A}_\mathcal{W}(\vec{\theta})$ that is considerably narrower than the actual primary beam of the telescope $\mathcal{A}(\vec{\theta})$. Figure 1 shows $\mathcal{A}_\mathcal{W}(\vec{\theta})$ for three different values of f $(2.0, 0.8$ and $0.6)$. For $f = 2.0$ we see that $\mathcal{A}_\mathcal{W}(\vec{\theta})$ is not very significantly different from $\mathcal{A}(\vec{\theta})$ in the region within the first null, the difference however increases in the first sidelobe and the sidelobe response is suppressed by a factor of 10 at $\mid \vec{\theta} \mid \approx 4^\circ$. We see that the effective primary beam gets narrower as the value of f is reduced. The value of $\mathcal{A}_\mathcal{W}(\vec{\theta})$ is a factor of ≈ 10 (100) lower compared to $\mathcal{A}(\vec{\theta})$ for $f = 0.8$ (0.6) at $\mid \vec{\theta} \mid = 2^\circ$ which corresponds to the boundary of the region within which the point sources have been subtracted. We see that, for $f = 0.8$ (0.6), tapering suppresses the first side lobe of $\mathcal{A}_\mathcal{W}(\vec{\theta})$ by a factor of $\approx 10^5$ (10^8) compared to $\mathcal{A}(\vec{\theta})$ at $\mid \vec{\theta} \mid = 4^\circ$. We expect the residual point source contribution to reduce by at least a factor of 10 and 100 for $f = 0.8$ and 0.6 respectively.

Figure 3 shows the angular power spectrum (C_ℓ) estimated from the residual visibility data using TGE with the f values $(2.0, 0.8$ and $0.6)$ discussed earlier. We see that in the absence of tapering we are able to recover the angular power spectrum of the diffuse synchrotron radiation at the low angular multipoles (large angular scales) $\ell < 3 \times 10^3$. The residual point source contribution is nearly independent of ℓ and has a value $C_\ell \approx 10$ mK^2 which dominates the estimated C_ℓ at the large angular multipoles (small angular scales) $\ell \geq 10^4$. We have a gradual transition from the diffuse synchrotron dominated to a point source dominated C_ℓ in the interval $3 \times 10^3 \leq \ell < 10^4$. The point source contribution comes down by a factor of more than 2 if we use the TGE with $f = 2.0$. We are now able to recover the angular power spectrum of the diffuse synchrotron radiation to larger ℓ values ($\ell < 5 \times 10^3$) as compared to the situation without tapering. The point source contribution, however, still dominates at larger ℓ values. We find that the point source contribution to C_ℓ is suppressed by more than a factor of 10 if we use TGE with $f = 0.8$ or 0.6. We are able to recover the angular power spectrum of the diffuse synchrotron radiation over the entire ℓ range using either value of f. The fact that there is no noticeable change in C_ℓ if the value of f is reduced from 0.8 to 0.6 indicates that a tapered sky response with $f = 0.8$ is adequate to detect the angular power spectrum of the diffuse synchrotron radiation over the entire ℓ range of our interest here.

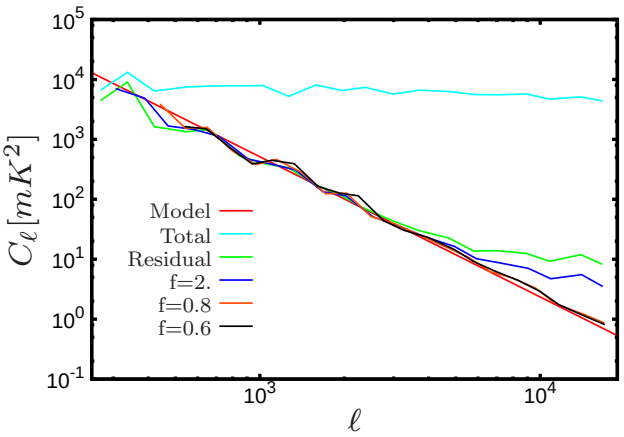

Figure 3. Angular power spectrum C_ℓ of total and residual data. It also shows the estimated C_ℓ using the TGE for the different values of f are also shown in the figure. In this figure the curves for $f = 0.6$ and 0.8 overlaps with each other.

The noise bias is an important issue in estimating the angular power spectrum, we illustrate this in Figure 4. For this purpose we have used a smaller frequency bandwidth of 8 MHz which increases the noise r.m.s. compared to the 16 MHz bandwidth used throughout the rest of the paper. Figure 4 shows C_ℓ estimated with the TGE with $f = 0.8$. We expect to recover the angular power spectrum of the diffuse synchrotron radiation over the entire ℓ range provided the noise bias is correctly estimated and subtracted out. Figure 4 shows the estimated C_ℓ in the situation where the noise bias is not subtracted. We see that the noise bias makes a nearly constant contribution of $C_\ell \approx 7.5$ mK^2 which dominates the estimated C_ℓ at large ℓ. It is necessary to subtract the noise bias in order to recover the C_ℓ of the diffuse radiation at large ℓ. Figure 4 demonstrates that the TGE correctly subtracts out the noise bias so that we are able to recover the C_ℓ of the diffuse radiation over the entire ℓ range.

6 SUMMARY AND CONCLUSION

It is difficult to model and subtract point sources located at the periphery of the telescope's field of view. These residual point sources pose a problem for estimating the power spectrum of the diffuse background radiation if all visible point sources are removed with high level of accuracy from inside the main lobe of the primary beam. For example, Pober et al. (2016) have recently shown the effect of the residual point sources outside the main lobe on estimating the power spectrum for MWA observation. This issue is discussed here in the context of measuring the angular power spectrum of the diffuse Galactic synchrotron radiation using

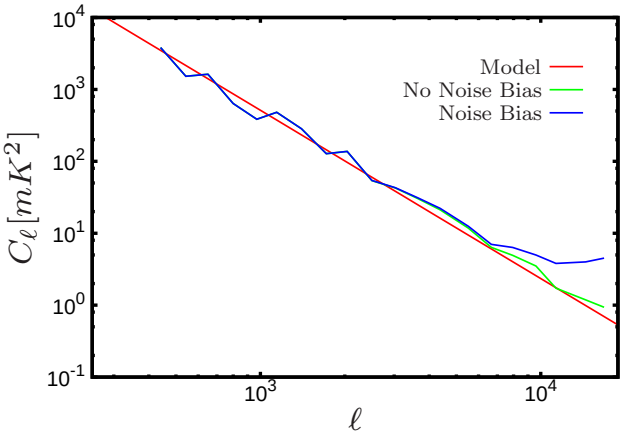

Figure 4. Angular power spectrum C_ℓ estimated using the TGE with $f = 0.8$. Results with the noise bias being present and with the noise bias subtracted are both shown here.

simulated 150 MHz GMRT observations. However, the same issue is also very important for detecting the EoR 21-cm power spectrum which is a much fainter diffuse signal that is not considered here.

It is possible to suppress the contribution from the residual point sources located at the periphery of the telescope's field of view through a frequency independent window function which restricts or tapers the sky response. The Tapered Gridded Estimator(TGE) achieves this tapering by convolving the measured visibilities with the Fourier transform of the window function. This estimator for the angular power spectrum has the added advantage that it internally estimates the noise bias from the measured visibilities and accurately subtracts this out to provide an unbiased estimate of C_ℓ. In this paper we demonstrate, using simulated data, that the TGE very effectively suppresses the contribution of the residual point sources located at the periphery of the telescope's field of view. We also demonstrates that the TGE correctly estimates the noise bias from the input visibilities and subtracts this out to give an unbiased estimate of C_ℓ.

The issues considered here are particularly important in the context of measuring the EoR 21-cm power spectrum. While all the different frequencies have been collapsed for the present analysis, it is necessary to consider the multi-frequency angular power spectrum $C_\ell(\nu_1, \nu_2)$ or equivalently the three dimensional power spectrum $P(k_\parallel, k_\perp)$ to quantify the 21-cm signal. We plan to generalize the TGE for this context in future work.

7 ACKNOWLEDGEMENTS

We would like to thank the anonymous referee for useful suggestions to improve this paper. SC would like to acknowledge the University Grant Commission, India for providing financial support through Senior Research Fellowship. SSA would like to acknowledge C.T.S, I.I.T. Kharagpur for the use of its facilities. SSA would also like to thank the authorities of the IUCAA, Pune, India for providing the Visiting Associateship programme. AG acknowledge the financial support from the European Research Council under ERC-Starting Grant FIRSTLIGHT-258942 (PI: L. V. E. Koopmans).

References

Ali S. S., Bharadwaj S.,& Chengalur J. N., 2008, MNRAS, 385, 2166A
Ali, Z. S., Parsons, A. R.,Zheng, H., et al. 2015, Ap.J, 809, 61
Bernardi, G., de Bruyn, A. G., Brentjens, M. A., et al. 2009, A & A, 500, 965
Begum, A., Chengalur, J. N., & Bhardwaj, S. 2006, MNRAS, 372, L33
Bhatnagar, S., Cornwell, T. J., Golap, K., & Uson, J. M. 2008, A & A, 487, 419
Bhatnagar, S., Rau,U., & Golap, K. 2013, Ap.J, 770, 91
Bowman J. D., Morales M. F., & Hewitt J. N. 2009, Ap.J, 695, 183
Chapman, E., Abdalla, F. B., Harker, G., et al. 2012, MNRAS, 423, 2518
Choudhuri, S., Bharadwaj, S., Ghosh, A., & Ali, S. S., 2014, MNRAS, 445, 4351
Choudhuri, S., Roy, N., Bharadwaj, S., Ali, S. S., Ghosh, A., & Dutta, P. 2016, submitted to MNRAS
Cornwell, T. J., & Perley, R. A. 1992, A & A, 261, 353
Cornwell, T. J.,Golap, K., & Bhatnagar, S. 2008, IEEE Journal of Selected Topics in Signal Processing, 2, 647
Datta, A., Bowman, J. D., & Carilli, C. L. 2010, Ap.J, 724, 526
Dillon, J. S., Liu, A., Williams, C. L., et al. 2014, PRD, 89, 023002
Dutta, P., Begum, A., Bharadwaj, S., Chengalur, J. N. 2007, MNRAS, 384, L34
Ghosh, A., Bharadwaj, S., Ali, S. S., & Chengalur, J. N. 2011a, MNRAS, 411, 2426
Ghosh, A., Bharadwaj, S., Ali, S. S., & Chengalur, J. N. 2011b, MNRAS, 418, 2584
Ghosh, A., Prasad, J., Bharadwaj, S., Ali, S. S., & Chengalur, J. N. 2012, MNRAS, 426, 3295
Iacobelli, M., Haverkorn, M., Orrú, E., et al. 2013, A & A, 558, A72
Intema, H. T., van der Tol, S., Cotton, W. D., et al. 2009, A & A, 501, 1185
Jelić, V., Zaroubi, S., Labropoulos, P., et al. 2008, MNRAS, 389, 1319
Kazemi, S., Yatawatta,S., Zaroubi, S., et al. 2011, MNRAS, 414, 1656
Liu, A., & Tegmark, M. 2012, MNRAS, 419, 3491
Liu, A., Parsons, A. R., & Trott, C. M. 2014a, PRD, 90, 023018
Liu, A., Parsons, A. R., & Trott, C. M. 2014b, PRD, 90, 023019
Mao, X.-C. 2012, Ap.J, 744, 29
Neben, A. R., Bradley, R. F., Hewitt, J. N., et al. 2015, Radio Science, 50, 614
Paciga, G., Chang,T.-C., Gupta, Y., et al. 2011, MNRAS, 413, 1174
Paciga, G., Albert, J. G., Bandura, K., et al. 2013, MNRAS, 433, 639
Parsons, A. R., Pober, J. C., Aguirre, J. E., et al. 2012, Ap.J, 756, 165
Parsons, A. R., Liu, A., Aguirre, J. E., et al. 2014, Ap.J, 788, 106
Platania, P.,Bensadoun, M., Bersanelli, M., et al. 1998, Ap.J, 505, 473

Pober, J. C., Parsons, A. R., Aguirre, J. E., et al. 2013, Ap.JL, 768, L36
Pober, J. C., Liu, A., Dillon, J. S., et al. 2014, Ap.J, 782, 66
Pober, J. C., Hazelton, B. J.,Beardsley, A. P., et al. 2016, arXiv:1601.06177
Seljak, U. 1997, Ap.J, 482, 6
Swarup, G., Ananthakrishnan, S., Kapahi, V. K., et al. 1991, Current Science, 60, 95
Thyagarajan, N., Udaya Shankar, N., Subrahmanyan, R., et al. 2013, Ap.J, 776, 6
Trott, C. M., Wayth, R. B., & Tingay, S. J. 2012, Ap.J, 757, 101
van Haarlem, M. P., Wise, M. W., Gunst, A. W., et al. 2013, A & A, 556, A2
Vedantham, H., Udaya Shankar, N., & Subrahmanyan, R. 2012, Ap.J, 745, 176